Available online at www.sciencedirect.com
ScienceDirect
Ceramics International 36 (2010) 2415–2420
CERAMICS INTERNATIONAL
www.elsevier.com/locate/ceramint

Multiferroic ceramics in $BaO–Y_2O_3–Fe_2O_3–Nb_2O_5$ system

Y.J. Wu *, S.P. Gu, Y.Q. Lin, Z.J. Hong, X.Q. Liu, X.M. Chen

Laboratory of Dielectric Materials, Department of Materials Science and Engineering, Zhejiang University, Hangzhou 310027, China

Received 20 January 2010; received in revised form 11 May 2010; accepted 20 June 2010
Available online 3 August 2010

Abstract

Multiferroic ceramics in $BaO–Y_2O_3–Fe_2O_3–Nb_2O_5$ system were synthesized and their dielectric, ferroelectric and magnetic properties were evaluated. XRD results showed that the ceramic composite consists of a major phase of tetragonal tungsten bronze structured $Ba_2YFeNb_4O_{15}$, and minor phases of monoclinic $YNbO_4$ and hexagonal $Ba_3Fe_2Nb_6O_{21}$. Three dielectric relaxations were observed in the temperature range from 125 to 575 K. The relaxor dielectric behavior in the temperature range from 125 to 350 K was attributed to the random occupation of Fe^{3+} and Nb^{5+} ions at B site of the tungsten bronze structure. The electrode polarization and the inhomogeneous structure contributed to the high-temperature and middle-temperature dielectric relaxations, respectively. Both the ferroelectric hysteresis loop and the magnetic hysteresis loop were measured, which suggested that the synthesized ceramic composite was a promising candidate of multiferroics.

Keywords: B. Composites; C. Dielectric properties; Magnetic properties

1. Introduction

The interesting physics and the potential applications in multifunctional devices have resurrected the research activities of multiferroic materials, which simultaneously exhibit at least two ferroic orders (ferroelectric, ferromagnetic, or ferroelastic) [1–3]. Multiferroic single-phase compounds are rare due to the mutual exclusive of the ferroelectric ordering and magnetic ordering, and most of them only exhibit multiferroicity at very low temperatures [4–7]. On the other hand, multiferroic composites, which incorporate both ferroelectric and magnetic compounds, typically demonstrate ferroelectric and magnetic ordering and larger magnetoelectric coupling response at room temperature [8–10]. Promising applications of these composites include magnetic field sensors, transducer, filters, oscillators, phase shifters, memory devices, and so on.

In the past decades, multiferroic composites consisting of ferroelectric ceramics and magnetic ferrites have been investigated in various systems, such as (a) piezoelectric ceramics (e.g., $Pb(Zr,Ti)O_3$, $BaTiO_3$, $Pb(Mg,Nb)O_3$, $(Sr,Ba)Nb_2O_5$) and ferrites, (b) piezoelectric ceramics and magnetic metals/alloys (e.g., Terfenol-D and Metglass), (c) piezoelectric ceramics and Terfenol-D and polymer, and so on [8–15]. In the simple 0–3 particulate ceramic composites, the interdiffusion and/or chemical reactions between the ferroelectric phases and ferrite phases during high-temperature sintering may deteriorate the properties of the ceramic composites. Moreover, large thermal expansion mismatch between them results in hard-sintering and leads to the formation of microcracks [8].

Recently, spark plasma sintering (SPS) with the merits of low sintering temperature and very short sintering time has been employed to fabricate fully dense multiferroic composites and avoid possible reactions between ferroelectric phases and magnetic phases [16–19]. By using the wet-chemical processing, *in situ* synthesis of multiferroic composites has been achieved and a three times larger magnetoelectric (ME) voltage coefficient was observed in the *in situ* synthesized samples [10]. The *in situ* synthesis of multiferroic composite was reported by Josse et al. in $Ba_2LnFeNb_4O_{15}$ (Ln = rare earth) system [20,21].

In the present paper, the *in situ* synthesis of multiferroic composite in $BaO–Y_2O_3–Fe_2O_3–Nb_2O_5$ system was investigated. The dielectric, ferroelectric and magnetic properties of the composite were evaluated.

* Corresponding author. Tel.: +86 571 87951410.
E-mail address: yongjunwu@zju.edu.cn (Y.J. Wu).

0272-8842/$36.00
doi:10.1016/j.ceramint.2010.07.022

2. Experimental

High purity $BaCO_3$, Y_2O_3, Fe_2O_3 and Nb_2O_5 were used as the raw materials. Stoichiometric mixture of the raw powders with nominal composition $Ba_2YFeNb_4O_{15}$ was ground in distilled water for 24 h in a ball mill with ZrO_2 balls. The grounded powders were dried and calcined at 1250 °C in air for 3 h and ball-milled again. The dried powders were pressed into cylindrical compacts of 12 mm in diameter and 1–2 mm in thickness under a pressure of 98 MPa with the addition of 5 vol% polyvinyl alcohol as binders. These compacts were then sintered from 1200 to 1300 °C in air for 3 h. Some samples were silver pasted or gold sputtered for dielectric and ferroelectric measurements.

Crystalline phases of the sintered ceramics were identified by powder X-ray diffraction (XRD) analyses (D/max 2550 PC, Rigaku Co., Tokyo, Japan). Data collection for Rietveld refinements was performed by 0.02° step with counting time of 2 s over the range of $2\theta = 5$–130°. The FULLPROF program was used for Rietveld structural refinement [22].

Dielectric properties were characterized in the temperature range from 125 to 570 K at 1 Hz–1 MHz with a broadband dielectric spectrometer (Turnkey concept 80, Novecontrol Technologies GmbH & Co. KG, Hundsangen, Germany). A ferroelectric test system (Premier II, Radiant Tech. Inc., NM, USA) was used for ferroelectric measurement at 1 Hz. Magnetization measurement was carried out with a magnetic property measurement system (MPMS-XL-5, Quantum Design, San Diego, CA, USA).

3. Results and discussion

Rietveld refinement of the XRD data of the sintered ceramic composite (hereafter referred to BYFN ceramics) was carried out in three phases model with a final difference and a profile fit in Fig. 1. The good agreement between the calculated and observed pattern with $R_p = 7.13\%$, $R_{wp} = 9.41\%$, $R_{exp} = 3.94\%$, and $\chi^2 = 5.70$ is observed. The refinement results demonstrate that the BYFN ceramics consist of three phases, $Ba_2YFeNb_4O_{15}$ (72.71(0.48) wt%), $YNbO_4$ (18.53(0.17) wt%) and $Ba_3Fe_2Nb_6O_{21}$ (8.76(0.10) wt%). The crystallographic data of the major phase of $Ba_2YFeNb_4O_{15}$ and structure refinement parameters are shown in Table 1. The major phase of $Ba_2YFeNb_4O_{15}$ has a tetragonal tungsten bronze structure with the space group *P4bm*. The unit cell parameters derived for $Ba_2YFeNb_4O_{15}$ were: $a = 12.58434(3)$ Å, $c = 3.98491(10)$ Å and the volume $V = 631.073(3)$ Å. Table 2 shows the atomic parameters of the proposed structure for the refinement, as well as the isotropic thermal parameters and relative occupancies. In the tetragonal tungsten bronze structure with a general formula $(A1)_2(A2)_4(C)_4(B1)_2(B2)_8O_{30}$: the trigonal interstices C are empty, the pentagonal interstices A1 are occupied by Y^{3+}, the tetragonal interstices A2 are occupied by Ba^{2+}, and the octahedral sites are statistically occupied by Fe^{3+} and Nb^{5+}. The $YNbO_4$ and $Ba_3Fe_2Nb_6O_{21}$ have monoclinic unit cell and hexagonal unit cell respectively.

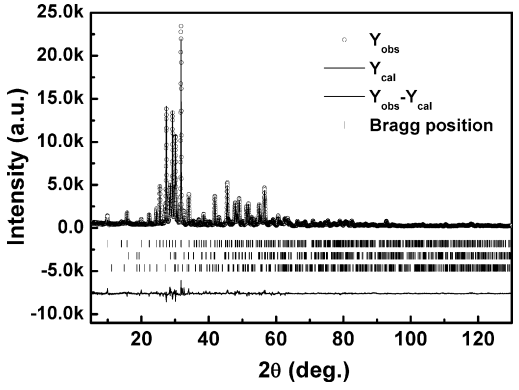

Fig. 1. Observed (open circles), calculated (solid lines), and difference (bottom line) of X-ray powder diffraction patterns for BYFN ceramics. The up, middle and bottom tick marks represent the position of all possible Bragg reflections of $Ba_2YFeNb_4O_{15}$ (72.71(0.48) wt%), $YNbO_4$ (18.53(0.17) wt%) and $Ba_3Fe_2Nb_6O_{21}$ (8.76(0.10) wt%) respectively.

Table 1
Crystallographic data and structure refinement parameters for $Ba_2YFeNb_4O_{15}$.

Crystallographic data	
Space group	*P4bm* (no. 100)
a (Å)	12.58434 (3)
c (Å)	3.98491 (10)
V (Å)	631.073 (3)
Data collection	
Temperature (°C)	25
Measuring range (°)	5–130
Step (2*θ*) (°)	0.02
Integration time (s)	2
Rietveld data	
Program	FULLPROF
Number of independent reflections	962
Number of independent parameters	48
Function for background level	Polynomial 5-order
Function for peak shape	Pseudo-voigt
($H^2 = U\tan^2\theta + V\tan\theta + W$)	
U	0.0785 (5)
V	−0.0287 (5)
W	0.0216 (6)
R_p (%)	7.15
R_{wp} (%)	9.43
R_{exp} (%)	3.95
χ^2	5.71

Fig. 2 shows the temperature dependence of the dielectric constant and dielectric loss of BYFN ceramics from 1 Hz to 100 kHz. Three dielectric relaxations with strong frequency dispersion are observed in the temperature range from 125 to 575 K. For description, the three dielectric relaxations are named as low-temperature (LT) dielectric relaxation, middle-temperature (MT) dielectric relaxation and high-temperature (HT) dielectric relaxation. The HT dielectric relaxations around 500 K disappear at frequency higher than 400 Hz, suggesting that this dielectric relaxation may be attributed to the electrode polarization. Fig. 3 shows the frequency dependence of the dielectric constant of BYFN ceramics with paste silver and sputtered gold contacts. Although the results from different measurements agree at high frequencies, the significant deviations at lower frequencies are observed. This confirms that the HT dielectric relaxation results from the electrode polarization.

Table 2
Atomic coordinates, isotropic thermal parameters and relative occupancies from XRD data for $Ba_2YFeNb_4O_{15}$.

Atom	Wyckoff position	x	y	z	Biso (Å^2)	Occupies
Y1	2a	0.00000(0)	0.00000(0)	0.00000(0)	0.022(6)	0.250(0)
Ba1	4c	0.17424(13)	0.67424(13)	0.98160(3)	4.904(8)	0.500(0)
Fe1	2b	0.00000(0)	0.50000(0)	0.50868(4)	3.791(12)	0.050(0)
Nb1	2b	0.00000(0)	0.50000(0)	0.50868(4)	3.791(12)	0.050(0)
Fe2	8d	0.07584(17)	0.21407(17)	0.46320(2)	2.648(6)	0.200(0)
Nb2	8d	0.07584(17)	0.21407(17)	0.46320(2)	2.648(6)	0.200(0)
O1	2b	0.00000(0)	0.00000(0)	0.00082(15)	1.292(2)	0.250(0)
O2	4c	0.28554(9)	0.78555(9)	0.56773(6)	1.292(2)	0.500(0)
O3	8d	0.07773(10)	0.21152(9)	0.01718(6)	1.292(2)	1.000(0)
O4	8d	0.32160(10)	0.01644(8)	0.59026(4)	1.292(2)	1.000(0)
O5	8d	0.14411(9)	0.08157(10)	0.43538(5)	1.292(2)	1.000(0)

The characteristic temperature of the MT dielectric relaxation shifts to higher temperatures and the magnitude of the dielectric constant decreases with increasing frequency. As shown in Fig. 2(b), the dielectric loss peak of the MT dielectric relaxation shifts to higher temperature with increasing frequency, indicating that the MT dielectric relaxation is thermally activated. The variation of $(\tan\delta)_{\max}$ of frequency versus $1000/T$ is shown in Fig. 4. This variation well follows the Arrhenius law:

$$f = f_0 e^{\frac{-E_a}{k_B T}} \quad (1)$$

where f_0 is the relaxation frequency at an infinite temperature, E_a is the activation energy, and k_B is the Boltzmann constant. The fitting parameters are $E_a = 0.45$ eV and $f_0 = 1.33 \times 10^9$ Hz. Considering its giant low frequency response and activation energy, the middle dielectric relaxation is most likely arises from the inhomogeneous structure, such as the interface between different phases or the grain boundaries.

The LT dielectric relaxation is clearly shown in the insets of Fig. 2. These curves illustrate a typical relaxor behavior where the dielectric constant decreases and the maximum dielectric constant temperature T_{max} shifts to high temperature with the increase of frequency, indicating a diffuse phase transition (DPT). The DPT can be described by modified Curie–Weiss

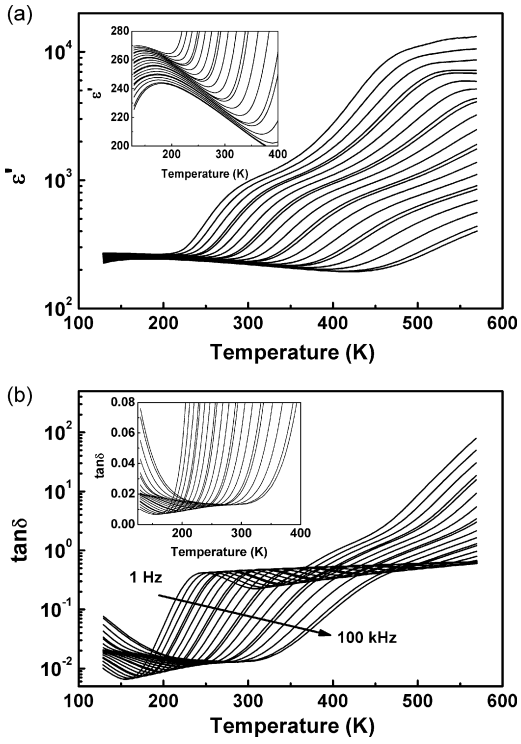

Fig. 2. Temperature dependence of dielectric constant and dielectric loss at various frequencies for BYFN ceramics. The insets show the low temperature (LT) dielectric relaxation.

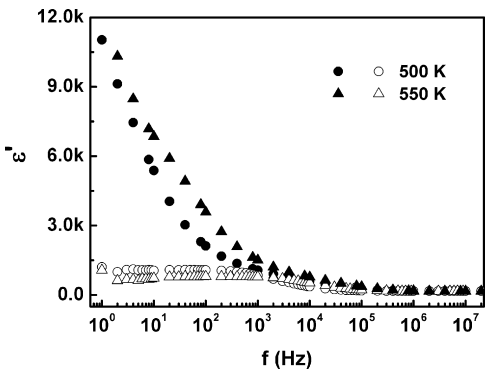

Fig. 3. Frequency dependence of dielectric constant of BYFN ceramics with silver-paint (solid symbols) and sputtered gold contacts (open symbols) at selected temperatures.

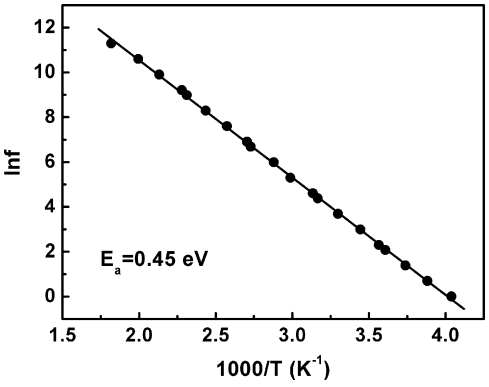

Fig. 4. Variation of $(\tan\delta)_{\max}$ of frequency versus $1000/T$ for middle-temperature dielectric relaxation of BYFN ceramics. Symbols are the experimental points and solid line is the Arrhenius fit.

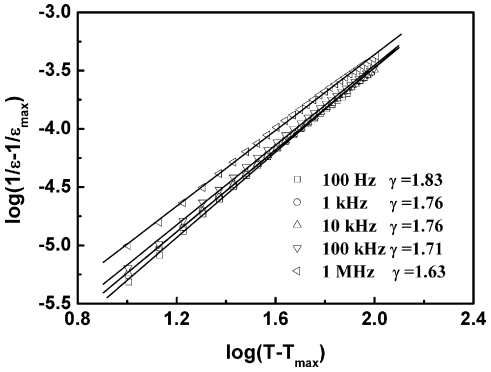

Fig. 5. Variations of $\log(1/\varepsilon - 1/\varepsilon_{max})$ with $\log(T - T_{max})$ at typical frequencies for BYFN ceramics. T_{max} is the temperature corresponding to the dielectric constant maximum, ε_{max}. Symbols are the experimental points and solid lines are the fitting lines.

law [23]

$$\frac{1}{\varepsilon} - \frac{1}{\varepsilon_{\max}} = \frac{(T - T_{\max})^{\gamma}}{C} \quad (2)$$

where ε is the dielectric constant, T is the temperature, ε_{max} is the maximum ε value at $T = T_{max}$, C is the modified Curie–Weiss constant and γ is an exponent that can vary from 1, for normal ferroelectrics to 1–2 for relaxor ferroelectrics. The variation of $\log(1/\varepsilon - 1/\varepsilon_{max})$ with $\log(T - T_{max})$ and the values of γ obtained from the slope of the curves at various frequencies are shown in Fig. 5. All the γ values are close to 2, confirming a typical relaxor ferroelectric behavior. In addition, the γ value slightly decreases with increasing frequency, which is not consistent with that of the well-known relaxor, such as $PbMg_{1/3}Nb_{2/3}O_3$ [23–25]. The dependence of γ value on the frequency has also been observed in other tungsten bronze compounds [26]. Further investigation is needed to explain this phenomenon. As shown in Fig. 6, the frequency dependence of T_{max} is found to be well obey the Vogel–Fulcher relation [27,28]

$$f = f_0 e^{\frac{E_a}{k_B(T - T_f)}} \quad (3)$$

where f_0 is the preexponential term, E_a is the activation energy for polarization fluctuation of an isolated micropolar region, T_{max} is the temperature of the dielectric constant maximum, k_B

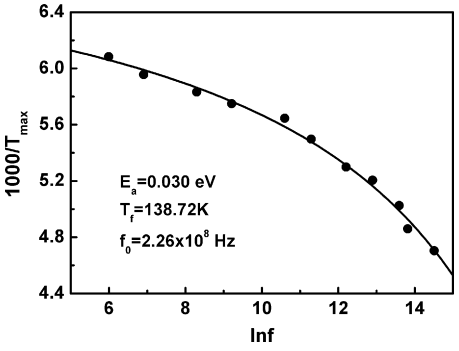

Fig. 6. Inverse of dielectric maximum temperature as a function of measurement frequency for BYFN ceramics. Symbols are the experimental points and solid line is the fitting line.

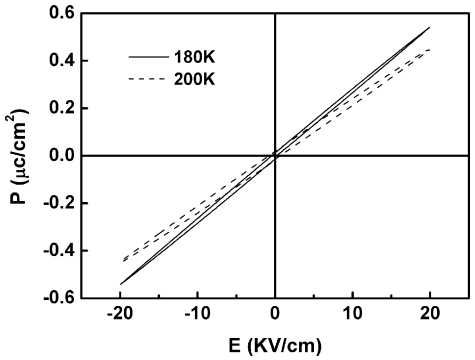

Fig. 7. *P–E* loops of BYFN ceramics measured at selected temperatures.

is the Boltzmann constant, and T_f is the Volgel–Fulcher temperature, i.e., the static freezing temperature. The value of E_a, T_f and f_0 for BYFN ceramics are found to be 0.030 eV, 138.7 K and 2.26×10^8 Hz, respectively.

The major phase of $Ba_2YFeNb_4O_{15}$ in BYFN ceramics possesses a tungsten bronze structure and the random occupation of Fe^{3+} and Nb^{5+} ions at B site is confirmed by the structure refinement (Fig. 1). The contribution of the cationic disorder at site A or site B to the diffuse, frequency dependence dielectric behavior has been reported by many authors [26,29–33]. Thus the relaxor dielectric behavior in the temperature range from 125 to 350 K of BYFN ceramics can be attributed to the random distribution of Fe^{3+} and Nb^{5+} ions at B site. The random distribution of Fe^{3+} and Nb^{5+} ions also causes the local compositional disorder and unequally distributed electrical charges, which lead to the appearance of micropolar regions by

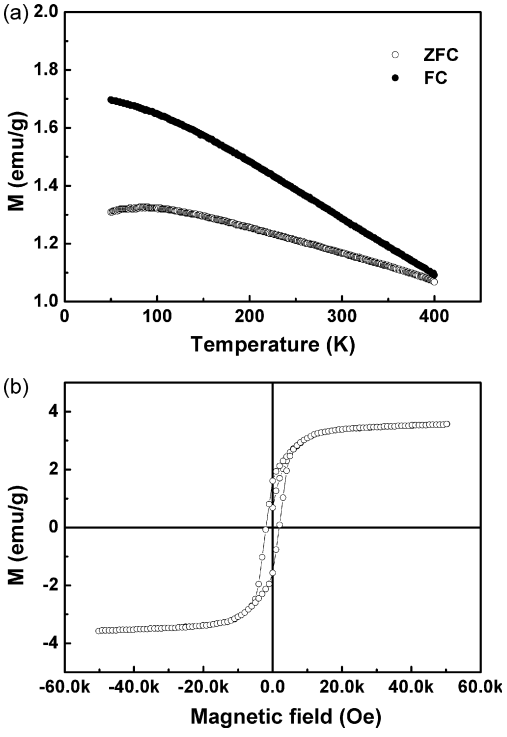

Fig. 8. (a) Magnetization curves of BYFN ceramics. FC and ZFC refer to field and zero-field cooling measurements. (b) *M–H* loop of BYFN ceramics at room temperature.

breaking the long-range polar order. As shown in Fig. 7, the ferroelectric hysteresis loops measured in the extended Curie region indicate that the micropolar clusters exist above $T_{\varepsilon_{max}}$ which is a typical ferroelectric-relaxor characteristic.

Magnetization curves of BYFN ceramics were measured at 1000 Oe by field and zero-field cooling and shown in Fig. 8(a). Fig. 8(b) shows the *M–H* loop of BYFN ceramics at room temperature. The value of remnant magnetization and coercive magnetic field is 1.609 emu/g and 2.010 kOe, respectively. The magnetic response of BYFN ceramics may be due to the presence of magnetically ordered Fe ion in $Ba_2YFeNb_4O_{15}$ and $Ba_3Fe_2Nb_6O_{21}$. As Fe^{3+} is paramagnetic, any Fe^{3+}–O–Fe^{3+} superexchange interactions will be antiferromagnetic in nature. In the distorted tungsten bronze structure, the change of the angle of Fe^{3+}–O–Fe^{3+} bond may result in the net magnetization in the BYFN ceramics [34]. The simultaneous observation of the ferroelectric and magnetic hysteresis loop reveals that BYFN composite is a promising candidate of composite multiferroics.

4. Conclusions

Ceramic composite consists of $Ba_2YFeNb_4O_{15}$, $YNbO_4$ and $Ba_3Fe_2Nb_6O_{21}$ was synthesized by the conventional solid-state reaction method. Three dielectric relaxations were observed in the temperature range from 125 to 575 K. The high-temperature and middle-temperature dielectric relaxation can be attributed to the electrode polarization and the inhomogeneous structure, respectively. The random distribution of Fe^{3+} and Nb^{5+} ions at B site of the tungsten bronze structure contributed to the relaxor dielectric behavior of BYFN ceramic at low temperatures. The observation of the ferroelectric hysteresis loop and the magnetic hysteresis loop suggests that the synthesized ceramic is a promising candidate of multiferroics.

Acknowledgment

The present work was supported by National Science Foundation of China under Grant Nos. 50872121 and 50832005.

References

[1] W. Eerenstein, N.D. Mathur, J.F. Scott, Multiferroic and magnetoelectric materials, Nature 442 (2006) 759–765.
[2] J. Wang, J.B. Neaton, H. Zheng, V. Nagarajan, S.B. Ogate, B. Liu, D. Viehland, V. Vaithyanathan, D.G. Schlon, U.V. Waghmare, N.A. Spaldin, K.M. Rabe, M. Wuttig, R. Ramesh, Epitaxial $BiFeO_3$ multiferroic thin film heterostructures, Science 299 (2003) 1719–1722.
[3] N. Hur, S. Park, P.A. Sharma, J.S. Ahn, S. Guha, S.-W. Cheong, Electric polarization reversal and memory in a multiferroic material induced by magnetic fields, Nature 429 (2004) 392–395.
[4] W. Prellier, M.P. Singh, P. Murugavel, The single-phase multiferroic oxides: from bulk to thin film, J. Phys.: Condens. Matter 17 (2005) R803–832.
[5] N.A. Hill, Why are there so few magnetic ferroelectrics, J. Phys. Chem. B 104 (29) (2000) 6694–6709.
[6] S.-W. Cheong, M. Mostovoy, Multiferroics: a magnetic twist for ferroelectricity, Nat. Mater. 6 (2007) 13–20.
[7] K.F. Wang, J.M. Liu, Z.F. Ren, Multiferroicity: the coupling between magnetic and polarization orders, Adv. Phys. 58 (4) (2009) 321–448.
[8] C.W. Nan, M.I. Bichurin, S. Dong, D. Viehland, G. Srinivasan, Multiferroic magnetoelectric composites: historical perspective, status, and future directions, J. Appl. Phys. 103 (2008) 031101.
[9] J. Ryu, A.V. Carazo, K. Uchino, H.E. Kim, Piezoelectric and magnetoelectric properties of lead zirconate titanate/Ni-ferrite particulate composites, J. Electroceram. 7 (1) (2001) 17–24.
[10] S.Q. Ren, L.Q. Weng, S.H. Song, F. Li, J.G. Wan, M. Zeng, $BaTiO_3$/$CoFe_2O_4$ particulate composites with large high frequency magnetoelectric response, J. Mater. Sci. 40 (2005) 4375–4378.
[11] J.G. Wan, H. Zhang, X. Wang, D. Pan, G. Wang, Magnetoelectric $CoFe_2O_4$–lead zirconate titanate thick films prepared by a polyvinylpyrrolidone-assisted sol–gel method, Appl. Phys. Lett. 89 (2006) 122914.
[12] C.W. Nan, L. Liu, N. Cai, J. Zhai, Y. Ye, Y.H. Lin, L.J. Dong, C.X. Xiong, A three-phase magnetoelectric composite of piezoelectric ceramics, rare-earth iron alloys, and polymer, Appl. Phys. Lett. 81 (2002) 3831–3833.
[13] C.W. Nan, G. Liu, Y.H. Lin, Influence of interfacial bonding on giant magnetoelectric response of multiferroic laminated composites of $Tb_{1-x}Dy_xFe_2$ and $PbZr_xTi_{1-x}O_3$, Appl. Phys. Lett. 83 (2003) 4366–4368.
[14] X.M. Chen, Y.H. Tang, I.W. Chen, Z.C. Xu, S.Y. Wu, Dielectric and magnetoelectric characterization of $CoFe_2O_4$/$Sr_{0.5}Ba_{0.5}Nb_2O_6$ composites, J. Appl. Phys. 96 (2004) 6520–6522.
[15] S.X. Dong, J.R. Cheng, J.F. Li, D. Viehland, Enhanced magnetoelectric effects in laminate composites of Terfenol-D/Pb(Zr,Ti)O_3 under resonant drive, Appl. Phys. Lett. 83 (2003) 4812–4814.
[16] Q.H. Jiang, Z.J. Shen, J.P. Zhou, Z. Shi, C.W. Nan, Magnetoelectric composites of nickel ferrite and lead zirconnate titanate prepared by spark plasma sintering, J. Eur. Ceram. Soc. 27 (2007) 279–284.
[17] Y. Shimojo, R. Wang, Y.J. Shan, H. Izui, M. Taya, Dielectric characters of $0.7Pb(Mg_{1/3}Nb_{2/3})O_3$–$0.3PbTiO_3$ ceramics fabricated at ultra-low temperature by the spark plasma sintering method, Ceram. Int. 34 (2008) 1449–1452.
[18] Y.J. Wu, J. Li, X.M. Chen, R. Kimura, K. Kakegawa, Effects of La_2O_3 addition and PbO excess on the transmittance of $PbZrO_3$–$PbTiO_3$–$Pb(Zn_{1/3}Nb_{2/3})O_3$ ceramics by spark plasma sintering, J. Am. Ceram. Soc. 91 (2008) 13–16.
[19] Y. Gao, Y.J. Wu, X.M. Chen, J.P. Chen, Y.Q. Lin, Y. Ma, Dense YMn_2O_5 ceramics prepared by spark plasma sintering, J. Am. Ceram. Soc. 91 (2008) 3728–3730.
[20] M. Josse, O. Bidault, F. Roulland, E. Castel, A. Simon, D. Michau, R. Von der Muhll, O. Nguyen, M. Maglione, The $Ba_2LnFeNb_4O_{15}$ "tetragonal tungsten bronze": towards RT composite multiferroics, Solid State Sci. 11 (2009) 1118–1123.
[21] E. Castel, M. Josse, F. Roulland, D. Michau, L. Raison, M. Maglione, In-situ formation of barium ferrite in iron-doped "tetragonal tungsten bronze": elaboration of room temperature multiferroic composites, J. Mag. Mag. Mater. 321 (2009) 1773–1777.
[22] J.R. Carvajal, Recent developments of the program FULLPROF, in commission on powder diffraction (IUCr), Newsletter 26 (2001) 12–19.
[23] K. Uchino, S. Nomura, Critical exponents of the dielectric constant in diffused-phase-transition crystals, Ferroelectrics 44 (1982) 55–61.
[24] V.V. Kirillov, V.A. Isupov, Relaxation polarization of $PbMg_{1/3}Nb_{2/3}O_3$(PMN) – a ferroelectric with a diffused phase transition, Ferroelectrics 5 (1973) 3–9.
[25] Z.R. Liu, Y. Zhang, B.L. Gu, X.W. Zhang, The properties of frozen local polarization in relaxor ferroelectrics, J. Phys.: Condens. Matter 13 (2001) 1133–1139.
[26] X.L. Zhu, X.M. Chen, X.Q. Liu, Dielectric abnormity of $Sr_4Nd_2Ti_4Nb_6O_{30}$ tungsten bronze ceramics over a broad temperature range, J. Mater. Res. 22 (2007) 2217–2222.
[27] H. Vogel, The law of the relation between the viscosity of liquids and the temperature, Phys. Zeit. 22 (1921) 645–646.
[28] G.S. Fulcher, Analysis of recent measurements of the viscosity of glasses, J. Am. Ceram. Soc. 8 (6) (1925) 339–355.
[29] R.E. Newnham, S. Rrolier-Mckinstry, K.M. Nair, J.P. Guha, A. Okamoto, Dielectric Ceramics: Processing, Properties and Applications, American Ceramic Society, Columbus, OH, 1993.
[30] C.A. Kirk, M.C. Stennett, I.M. Reaney, A.R. West, A new relaxor ferroelectric, $Ba_2LaTi_2Nb_3O_{15}$, J. Mater. Chem. 12 (2002) 2609–2611.

[31] J. Ravez, A. Simon, Some solid state chemistry aspects of lead-free relaxor ferroelectrics, J. Solid State Chem. 162 (2001) 260–265.
[32] Y. Yuan, X.M. Chen, Y.J. Wu, Diffused ferroelectrics of $Ba_6Ti_2Nb_8O_{30}$ and $Sr_6Ti_2Nb_8O_{30}$ with filled tungsten–bronze structure, J. Appl. Phys. 98 (2005) 084110.
[33] X.L. Zhu, X.M. Chen, X.Q. Liu, Y. Yuan, Dielectric characteristics and diffuse ferroelectric phase transition in $Sr_4La_2Ti_4Nb_6O_{30}$ tungsten bronze ceramics, J. Mater. Res. 21 (2006) 1787–1792.
[34] S.K. Patri, R.N.P. Choudhary, M. Manivel Raja, $La_2Bi_3Fe_5Ti_3O_{27}$: structural, electrical and magnetic properties, J. Alloy Compd. 478 (2009) 9–13.